OPTICAL PROPERTIES OF FLYASH

Contract No. DE-AC22-87PC 79903

Quarterly Report for Period 1 July – 30 September 1991

Prepared for Pittsburgh Energy Technology Center

Principal Investigator Professor S. A. Self

November 1991

HIGH TEMPERATURE GASDYNAMICS LABORATORY
Mechanical Engineering Department
Stanford University

DOE/PC/79903--T10

DE92 005493

OPTICAL PROPERTIES OF FLYASH
Contract No. DE-AC22-87PC 79903
Quarterly Report for Period 1 July – 30 September 1991
Prepared for Pittsburgh Energy Technology Center
Principal Investigator Professor S. A. Self

EXECUTIVE SUMMARY

The general aims of this research are to provide a fundamental scientific basis for the physical understanding and reliable calculation of radiative heat transfer in coal combustion systems, particularly as it is influenced by the presence of inorganic constituents deriving from the mineral matter in coal.

The work is organized under four tasks. Tasks I and II were initiated in October 1987; Tasks III and IV were funded from October 1988.

Task 1. Characterization of Flyash: Under this heading the chemical composition and size distribution of representative flyashes are being measured by appropriate microanalytical techniques to provide information required in Task 2.

Task 2. Measurements of the Optical Constants of Slags: Under this heading measurements of the infrared optical constants (i.e., the complex refractive index $m = n - ik$) of synthetic slags are being made as a function of wavelength and temperature for controlled compositions. Particular attention will be given to the contribution of the Fe_2O_3 content and its valence state. The data is being reduced to yield formulae giving the complex refractive index over relevant ranges of wavelength and temperature, as a function of the relevant metal oxide constituents.

Task 3. Sample Calculations of the Radiant Properties of Flyash Dispersions: This component comprises various calculations to guide and evaluate the experimental work under the other three tasks.

Task 4. Measurement of the Radiant Properties of Flyash Dispersions: This bench-scale experiment is planned to compare the measured radiant properties of a dispersion of well-characterized ash with computations based on data developed under the first two tasks.

In this sixteenth quarter good progress has been made under Tasks 2 and 4, as reported in the Quarterly Report, and summarized below. Tasks 1 and 2 are now essentially complete apart from writing of a comprehensive report. Some further computations are planned under Task 3 while a series of measurements remain to be made under Task 4.

Task 1

The ashes being characterized are samples from power plants or pilot-scale combustors derived from combustion of six of the coals selected for study under the parallel PETC program on "Transformation of Inorganic Coal Constituents in Combustion Systems."

The principal features requiring characterization are particle size and composition distributions, including correlations between size and composition. Size distributions are being measured in house by Coulter counter. Size and composition distributions are being determined by automated SEM/microprobe analysis at UNDERC. Other in-house characterization work under way includes size classification by wet sieving combined with classification by density using flotation/sedimentation techniques, low temperature ashing for the char content and magnetic separation for the magnetite content resulting from combustion of pyrite.

Size distributions for all six ashes over the range 0.5 – 60 μm have been completed using the Coulter multisizer with a technique employing two orifices to cover the whole range. A suitable technique for matching distributions using two orifice sizes was devised. The measured distribution was found to be very well represented by truncated log-normal distributions. Comparison with the size distribution from automated SEM shows some discrepancy which is still being investigated.

Micrographs of the ash samples prepared by UNDERC for automated SEM/EDX size-composition analysis revealed many agglomerates, casting some doubt on the validity of the data. A freeze-drying technique for sample preparation has been developed at Stanford which gives very well dispersed samples. The automated SEM/EDX analysis has been repeated using such samples and the results have been analyzed using statistical computer codes developed at Stanford. Ternary diagrams of the composition distributions (in color) have been prepared using software developed at Stanford. In the past quarter, automated SEM/EDX analyses have been completed and analysis of the data made for all six ashes.

In addition, density classification results have been obtained for all six ashes and compared with results from SEM analysis for composition, which, of course, determines the density. Currently, size distributions are being determined for the density-separated fractions to obtain composition/size correlations for comparison with the SEM/EDX data. This task is now essentially completed.

Task 2

Methods for determining the infrared optical properties of solid synthetic and natural slags at low temperatures have been established in prior work at Stanford. In the present work the main effort has been devoted to the development of suitable apparatus and techniques for performing similar measurements on slags at temperatures to 2000K, when the slag is liquid. Basic experimental strategies have been decided and apparatus has been designed to accomplish this task. Tests at high temperatures during past quarters have resulted in the first reliable measurements of the infrared absorption of liquid slag.

Two complementary techniques involving infrared optical measurements on liquid samples of synthetic slag maintained in an electric furnace have been developed. The first, for the wavelength range 1 – 5 μm where the absorption index is low ($k \leq 10^{-2}$) employs a submerged platinum mirror to measure the absorption of thin films of slag by a double-pass technique. The second, applicable over the whole wavelength range (1–12 μm), measures the surface reflectance of the liquid slag relative to that of a cold gold mirror in an external reference path.

The first technique has been successfully used to obtain the first reliable measurements of the infrared absorption of liquid slag (at 2000 K).

Efforts have since been concentrated on developing and testing the second technique (for surface reflectivity measurements). It was determined that the quality of the data obtained is limited by the differing absorptions due to CO_2 and H_2O in the hot measurement path and the cold reference path. To eliminate this problem, the whole apparatus has been enclosed in a chamber, purged with dry nitrogen.

With this modification, good measurements of the reflectivity of synthetic slag containing 5% Fe at 1600°C were made over the whole wavelength range 1–12 μm. The data in the range 8–12 μm were reduced, using the Kramers–Kronig technique to give both the real and imaginary parts of the complex refractive index.

Possible sources of uncertainty in these measurements have been critically investigated and resolved. In particular, a problem due to contamination of a mirror by furnace gases has been identified and steps taken to eliminate it by redesign of the optical system. Reflectance measurements on liquid slags containing zero, 1%, 5%, 10% and 20% iron (as Fe_2O_3) have been completed. The results have been reduced, using Kramers-Kronig analysis to yield the real (n) and imaginary (k) parts of the complex refractive index.

Measurements are currently underway on liquid slags of varying SiO_2 composition. When completed Task 2 will be essentially completed.

Task 3

Programs have been written for Mie scattering calculations which are then convolved with input on the size and optical constants distributions for a particulate dispersion to yield the spectral scattering and absorption coefficients of the aerosol. Additionally, a program has been written to solve the radiation transfer problem for a homogeneous slab, utilizing the exact solution method of Case's normal modes. Input for the spectral scattering and absorption coefficients from the first program allows the spectral scattering, absorption and emission properties of the slab to be computed. These can then be integrated over wavelength to yield the total radiative heat transfer characteristics of the slab.

These programs have been used to determine the importance of certain features of typical ashes for radiation transfer. These include the sensitivity of the optical/radiative properties of a flyash dispersion to (i) composition-size correlation, especially with regard to the distribution of iron oxides with particle size, and (ii) the presence of bubbles in the glassy ash particles.

This computational capability is also being used to evaluate the experimental conditions in the design of the apparatus for Task 4.

Task 4

Careful consideration has been given to the feasibility of various basic approaches for implementing the goals of this task. After evaluating various experimental techniques, a basic approach has been identified, which involves extinction measurements on flyash dispersed in suitable organic liquids. Measurements of the infrared transmission of three selected liquids have been made which confirm their suitability for this purpose. CaF2 windows for an absorption cell have been acquired and preliminary tests of a suitable cell design have been made.

During the past quarter, careful consideration has been given to the detailed optical design of a transmissometer for measurements on flyash dispersions in infra-red transmitting liquids.

Now that Task 2 is completed, the infra-red optical system is being re-configured for the experimental phase of Task 4.

1.0 INTRODUCTION

This is the sixteenth quarterly report under DOE contract No. DE-AC22-87PC 79903 entitled "Optical Properties of Flyash." Tasks 1 and 2 of this program were funded from 15 September 1987. Tasks 3 and 4 were funded from 15 September 1988.

The general aims of this research are to provide a fundamental scientific basis for the physical understanding and reliable calculation of radiative heat transfer in coal combustion systems, particularly as it is influenced by the presence of inorganic constituents deriving from the mineral matter in coal. Some preliminary work in this area has been carried out at Stanford in the past several years with NSF support. The present program will greatly enlarge the scope of this work.

The complete, integrated program of theoretical and experimental work comprises four separate tasks.

Task 1. Characterization of Flyash

Task 2. Measurements of the Optical Constants of Slags

Task 3. Sample Calculations of the Radiant Properties of Flyash Dispersions.

Task 4. Measurements of the Radiative Properties of Flyash Dispersions.

In Task 1, the chemical composition and size distribution of representative flyashes are being measured by appropriate microanalytical techniques to provide information required in Tasks 2 and 3.

In Task 2, measurements of the infrared optical constants (i.e., the complex refractive index $m = n - ik$) of synthetic slags are being made as a function of wavelength and temperature for controlled compositions. Particular attention is being given to the contribution of Fe_2O_3 content and its valence state. The data will be reduced to yield formulae giving the complex refractive index over relevant ranges of wavelength and temperature, as a function of the relevant metal oxide constituents.

In Task 3, sample calculations are being made for typical ash loadings, size distributions and compositions for simple geometries, with two main purposes: first, to provide insight and physical understanding of the role of flyash in radiative heat transfer in combustion systems; second, to indicate the sensitivity of the results to the characteristics of the input data. Such calculations will also be used to determine appropriate conditions and to predict the expected measured radiative properties for the experiment of Task 4.

The experiment of Task 4 is designed to critically test our ability to predict the measured spectral emittance and scattering coefficient of flyash dispersions under well-controlled laboratory conditions utilizing the optical property data developed in Task 2. Particular attention will be paid to assessing the contribution of the char component in typical ashes. Any discrepancies between calculated and measured quantities revealed by these tests will be resolved by appropriate further studies.

A more detailed description of the scope of these tasks is given below. First, however, an outline is given of the rationale for the overall approach adopted in this program.

1.1 Rationale of Overall Approach

To account for the effects of flyash in radiative heat transfer calculations requires a knowledge of the contributions of the ash to the spectral absorption (a_λ) and scattering (σ_λ) coefficients of the particulate dispersion, together with the phase function Φ_λ describing the anisotropy of the scattering. These quantities depend on the particulate loading as well as the distributions of the size and optical properties of the particles.

For a spherical particle of homogeneous, optically isotropic material, characterized by a complex refractive index $m \equiv (n - ik)$ Mie theory allows one to compute the spectral absorption ($Q_{\lambda,a}$) and scattering ($Q_{\lambda,s}$) efficiencies of the particle, as well as the phase function ϕ_λ. For randomly polarized radiation, these quantities are a function of the particle size parameter $x \equiv (\pi d/\lambda)$, and the complex refractive index $m(C, \lambda, T)$, a function of composition, wavelength and temperature.

For a monodispersion of identical spherical particles, of specified loading (i.e. number density), the particulate's contribution to the optical properties (a_λ, σ_λ and Φ_λ) of the medium are simply related to the spectral properties ($Q_{\lambda,a}$, $Q_{\lambda,s}$, ϕ_λ) of a single particle. It is also straightforward to compute the spectral optical properties of the medium for a polydispersion of spheres of identical composition, by convolving the results of Mie calculations for spheres of varying diameter (i.e. x) for fixed wavelength (and hence fixed m), with the particle size distribution (assumed given). In the case of a particulate material, like flyash, for which it is reasonable to assume that individual particles are of homogeneous composition but the composition varies from particle to particle, it is still possible to compute the spectral characteristics of the particulate dispersion by dividing the particles into an appropriate number of classes of varying composition (and hence m), each having a specified size distribution, and summing over particle classes.

In radiative heat transfer calculations, the contribution of the gas to the spectral absorption coefficient is added to that of the particles to obtain the combined optical properties of the medium on a spectral basis. These optical properties are then used as input for a radiation transfer code to calculate radiative fluxes, on a spectral basis, for a particular combustor geometry and boundary conditions. Finally, to obtain total heat transfer quantities such as the overall radiant heat flux, integrations over wavelength must be made.

The procedure, outlined above, represents the only logical approach to the computation of radiative heat transfer in flyash laden combustion gases. To implement this procedure requires, as input, a detailed characterization of the ash with respect to its size and (complex) refractive index distributions on a spectral basis.

Now, while techniques are available for determining the size distribution of powder samples, such as flyash, there are no practical means available for reliably determining the complex refractive index distribution of a complex material such as flyash either on a single particle basis, as a powder or as a dispersed aerosol. However, it is possible, using modern microanalytical techniques, specifically computer-automated SEM/EDX analysis, to determine the size and chemical composition of a heterogeneous powder on a particle by particle basis for a statistically large number of particles.

If the compositions of individual particles can be related to the complex refractive index of their material, then the characterization of a particular ash in terms of its size and composition distributions can lead to the necessary input for carrying out the calculations, outlined above, to compute radiation transfer in combustion systems containing that ash.

Thus the key requirement, necessary for the implementation of this approach, is data on the optical constants (i.e. the components n, k of the complex refractive index) as a function of composition, wavelength and temperature covering the range of compositions found in representative ashes. Since, as noted above, and emphasized in texts on the optical properties of particulate matter, it is impractical to extract reliable data on the optical constants of material in particulate form, the only viable approach is to make measurements on homogeneous bulk samples for which well-established techniques are available.

The foregoing arguments provide the rationale for the present program. Characterization of representative flyashes concerning their size and composition distributions constitutes Task 1, while measurements of the optical constants on bulk samples of synthetic slags as a function of relevant ranges of composition, wavelength and temperature constitute Task 2. Task 3 is designed to provide computational capabilities to support the other tasks, while Task 4 is planned to provide an experimental test that the measured optical properties of a dispersion of flyash can indeed be computed reliably from a knowledge of the size and composition distributions of the ash.

1.2 Description of Tasks

TASK 1 - Characterization of Flyash

Extensive prior analyses of flyash from a wide range of coals plus analyses of the mineral matter in raw coals, together with knowledge of the transformation processes occurring during combustion, lead to the following overall picture of the nature of flyash.

The particle size distribution is very broad with a volume (or mass) mean diameter on the order of 10 μm. Typically it is well represented by a log normal distribution with the 1% and 99% sizes in a cumulative plot by volume occurring at ~1 μm and 70 μm respectively. Evidence of a distinct submicron fume due to homogeneous condensation of volatile mineral matter is sometimes found, but this fraction can be expected to contribute negligibly to radiation transfer.

With regard to chemical composition, several distinct classes of particle can be identified and plausibly related to their origin and formation mechanisms.

By far the preponderant class, usually representing on the order of 90% or more of the ash on a mass basis, consists of vitreous (amorphous) material composed primarily of SiO_2, Al_2O_3, CaO and MgO, usually in that order, but containing varying smaller percentages of other metal oxides, notably Fe_2O_3. It can appropriately be identified as particles of impure (calcium) aluminosilicate glass derived from the microscopic clay-like mineral inclusions in the coal matrix. As char burnout proceeds these inclusions melt and form liquid globules on the surface of the char (which they do not wet) and are then released into the gas.

These glassy particles tend to be quite spherical with smooth surfaces and of reasonably homogeneous composition as is to be expected from their formation as liquid droplets. As they cool after release from the char surface, they remain in the vitreous state because the cooling rate is much faster than the crystallization rate for the formation of specific phases. The fact that the bulk of most ashes consists of reasonably spherical, homogeneous and vitreous (and therefore optically isotropic) particles is a very fortunate fact, since they satisfy the assumptions of the Mie theory remarkably well.

Micrographs of optically polished sections of ash cast in epoxy resin, shows that these glassy particles sometimes contain a number of small bubbles of gas evolved from the char and trapped in the particles as they form on the char surface. More rarely, large, thin-walled cenospheres are observed which presumably are "glass-blown" when a liquid drop covers a pore in the char from which a relatively large volume of gas is evolved under pressure. Although such cenospheres are very prominent objects in micrographs, their number is usually too small to significantly affect radiation transfer.

Auger spectroscopic studies of ash often show a thin surface layer composed of volatile metals and high in sulfur (as sulfates) and water. The presence of a thin layer of adsorbed water containing sulfate ions controls the electrical resistance of the surface which is very important in the performance of electrostatic precipitators. However, this surface layer, of different composition from the underlying particle, is too thin (≤100Å) relative to wavelengths of interest to affect the optical properties of the particle.

Apart from this major class of glassy particles, several distinct minor classes of particle types can be identified, each comprising, at most, a few percent by mass of the flyash. One such class consists of incompletely burned char particles which are clearly identified in optical and SEM micrographs by the fact that they are black, of irregular shape and porous. The mass fraction of char depends on the particular coal and the combustor configuration and operating conditions. In modern combustors the mass fraction of unburned char is normally a few percent at most.

Another minor class consists of particles of adventitious incombustible mineral matter (e.g. quartz) which is contained in the pulverized coal feed. Such particles are usually large and of irregular shape, often showing rounded edges indicating partial melting.

A third minor class consists of magnetite (Fe_3O_4) which derives from the combustion of pyrite (FeS_2) particles contained in the coal grind. These magnetite particles are black, generally spherical, magnetic and much denser than the glassy particles. The proportion of magnetite particles depends on the coal type, being largest in high sulfur coals, because the sulfur is mostly associated with pyrite. Recent work has shown that much of the pyrite in the coal grind can be removed by washing/sedimentation with a reduction in SO_x emissions as high as 50% in some high sulfur coals.

The ashes selected for characterization are samples from power plants or pilot-scale combustors derived from the same seven coals selected for study under the parallel PETC program on "Transformation of Inorganic Coal Constituents in Combustion Systems" which comprise four bituminous, one sub-bituminous and two lignite coals.

A variety of techniques are being used in the characterization of these ashes. The principal method for determining size distributions employs a Coulter Multisizer which is capable of giving accurate, reliable results of high resolution over a wide dynamic range ≤1 μm to ≥ 100 μm.

Automated, computer-controlled, combined SEM/EDX microanalysis will be the principal technique used to determine the distributions of composition and size for a large number (~1000) of particles for each ash. The size distributions will be compared with those obtained by the Coulter counter.

Other techniques to be used include classification by density using liquids of varying density in a centrifuge, together with classification by size using a wet-sieving method. These techniques can yield density and size separated fractions for further examination by microanalytical techniques such as energy-dispersive X-ray spectroscopy. In addition, the magnetite particles may be separated by magnetic separation. The char content will be determined by low temperature ashing.

TASK 2 - Measurements of Optical Constants of Synthetic Slags

This task is planned to provide the basic optical properties data in a comprehensive and conveniently usable form. The optical constants (i.e., the components of the complex refractive index $m = n - ik$) of samples of synthetic slags of controlled compositions will be measured using established techniques involving transmission and surface reflectance methods. The wavelength range will extend from the visible to 12 μm, and the temperature range will extend to 2000K.

In earlier work at Stanford, supported by NSF, extensive measurements of this type were made on polished wafers of synthetic slags at temperatures up to 1200 K. A major component of this task will be to extend such measurements to higher temperatures (~2000 K) where the slag is liquid. This requires the development of modified techniques which present a number of more or less severe technical challenges.

Initially, the optical constants of the basic calcium-aluminosilicate host glass will be determined for the composition range defined by Task 1. Subsequently, by adding infrared-active mineral oxide constituents in controlled amounts, one at a time, the modifications to $m(\lambda, T)$ produced by such constituents will be quantitatively determined. The particular constituents (and their range of mass fractions) to be examined will be determined by those disclosed by Task 1, taking account of knowledge of the optical activity at relevant wavelengths of such additions from the literature of glass technology. Specific constituents to be examined will include Fe_2O_3, taking especial account of its valence state (Fe^{2+}/Fe^{3+} ratio), and of TiO_2. The contribution of the OH radical to the optical properties will be evaluated and quantified if significant.

The experimental data on $m(\lambda, T)$ as a function of composition, over the range relevant to coal ashes, will be reduced to generate simple correlation formulae. The latter will constitute the data base necessary to calculate the radiative properties of bulk slags and ash dispersions required for understanding and computing radiative transfer in coal combustion systems.

TASK 3 - Sample Calculations of the Radiant Properties of Flyash Dispersions

This task is intended to provide computational capabilities to support the other tasks. It includes the following components.

(i) A Mie scattering code to calculate the absorption and scattering efficiencies and phase function of a single sphere of specified size parameter and complex refractive index. A modified Mie code will also allow such computations for hollow spheres.

(ii) A code to convolve the results from (i) over a specified size distribution and loading to compute the absorption and scattering coefficients and phase function of a homogeneous polydispersion.

(iii) A code to sum the results of (ii) for a number of classes of particles of varying refractive indices and size distributions, i.e. for a heterogeneous polydispersion.

(iv) A radiation transfer code to calculate the absorption, scattering and emission characteristics of a homogenous, isothermal slab of dispersed ash on a spectral basis.

(v) A code to integrate the spectral results from (iv) over wavelength to yield the total radiative properties of the slab.

Calculations using these codes will be used to provide sensitivity analyses to guide the characterization work of Task 1, and to design and evaluate the results of Task 4.

TASK 4 - Measurement of the Radiative Properties of Flyash Dispersions

The purpose of this laboratory scale experiment is to test our ability to predict the measured radiative properties of a dispersion of well-characterized flyash. As such it will provide a critical test of the effectiveness of the overall approach adopted in this program.

2.0 PROGRESS IN THE PAST QUARTER

2.1 Task 1: Characterization of Fly Ash

Task 1 was completed two quarters ago. A paper based on the work, titled "Size Distributions of Fly Ashes by Coulter Multisizer: Use of Multiple Orifices and Fitting to Truncated Log-normal Distributions," has been submitted to Aerosol Science and Technology for publication. It is also being issued as a technical memorandum.

2.2 Task 2: The Optical Properties of High Temperature Slag

The immediate goal of this task is to measure the high temperature optical properties of coal slag. The complex refractive index, $m = n + ik$, is being measured for synthetic slags at high temperatures, near 1900 K. The effect of composition on the optical properties is also being investigated.

In previous QPR's, measurements of the near normal reflectance of nine slag compositions were reported (SA00, SA01, SA05, SA10, SA20, SA4S, SA2S, SA1S, and NAEB). From those measurements the complex refractive index, m, was computed using the Kramers–Kronig relations, with n being determined for the wavelength range $1 < \lambda < 13\mu m$ and k being determined for a narrower range ($8 < \lambda < 13\mu m$). These nine slags span a range of compositions similar to those found for most (by volume) ash particles under Task 1.

As reported in the previous (7-1991) QPR, transmittance measurements were completed for three slags (SA01, SA4S, and SA05). The transmittance was measured in the wavelength range $1 < \lambda < 5\mu$m, where the Fe_2O_3 in the slag causes absorption of the infrared radiation. These measurements conclude Task 2, and provide sufficient information for determining the radiative properties of fly ash dispersions.

2.2.1 Scheduled Activities

Task 2 is now complete apart from final correlation with composition and with room temperature data. During the next quarter efforts will be focused on this analysis, further heat transfer analysis using codes developed under Task 3, and preparation of the final report.

2.3 Task 3: Sample Calculations of the Radiant Properties of Fly Ash Dispersions

The goals of this task are to provide sample calculations which allow estimates of the influence of fly ash on the total radiative heat transfer in coal combustors and provide computational capabilities required to evaluate our overall approach using results from Task 4.

2.3.2 Overview

In this research program, we have adopted the approach that by measuring fundamental properties (i.e, the complex refractive index, m) of the fly ash which participates in the radiation transfer, one can use well established theoretical principles (Mie theory) to compute the radiative properties of dispersions of fly ash as found in coal combustors. With this approach one can understand the underlying principles that affect the radiative properties of an ash dispersion and more confidently predict how variations in the characteristics of the ash dispersion cause variations in its radiative properties.

An important criterion in this approach is that the fly ash particles be spherical, homogeneous, and isotropic. Fortunately, fly ash particles are formed at high temperatures at which most of them are molten, leading primarily to spherical particles. Furthermore, one should expect that molten particles will be reasonably homogeneous and isotropic. On cooling, most fly ash particles form glassy spheres which are homogeneous and isotropic, but some, and perhaps most from some types of coal, may form spheres or spheroids with interior bubbles or voids.

To the extent that some ash particles are not spherical, homogeneous, or even isotropic, one should consider departures from the simpler model as corrections. The importance of these corrections must be weighed in light of the overall influence of ash on radiation heat transfer in coal combustors. We expect that most fly ash is well modeled as isotropic, homogeneous spheres, and that this approach goes much further toward explaining the effects of fly ash on radiative transport than other possible approaches.

2.3.3 Progress

Computer codes have been developed which calculate the radiative properties of fly ash dispersions using fundamental data obtained from Tasks 1 and 2. During the previous quarter, these codes were used to study the sensitivity of the transmittance of ash dispersions (Task 4) to loading and ash optical properties. See the discussion under Task 4 for details.

During the previous quarter new computer codes have been developed for computing the radiative transfer through a planar slab of CO_2, H_2O, and fly ash in radiative equilibrium, that is, assuming the only mode of heat transfer is radiation transfer. As a result, the temperature throughout the slab is determined by the radiant flux. This limit is in some sense[1] the opposite extreme of the uniform temperature slab solution.

The temperature distribution and heat flux was computed for four cases: 1) a one meter slab with gas only, 2) a one meter slab with gas and fly ash, 3) a three meter slab with gas only, and 4) a three meter slab with ash and fly ash. The boundaries were assumed to be black with one boundary (at $x = L$) at 1000 K and one boundary (at $x = 0$) at 2000 K. The heat flux, Q, is normalized by the heat flux one would get if no ash or gas was present, thus $Q = 1$ is the maximum heat flux. The results demonstrate the strong shielding capability of fly ash, where adding fly ash to the three meter slab reduces the heat flux from 0.780 to 0.582. The consequence to coal combustors is that the ash will cause the ash and gases to cool more slowly when more fly ash is present.

2.3.4 Radiative transfer for a medium in radiative equilibrium

When the heat transfer through a medium is due to radiative transfer only, i.e., a medium in radiative equilibrium, the temperature of the medium is determined by the net radiative energy flowing through each position in the medium. In the optically thin limit the temperature is only weakly coupled to the temperatures of the boundaries of the medium, and the heat flux through the medium is high, approaching the limit

1. The radiative equilibrium solution is the solution when there is no convection or conduction heat transfer, while the uniform temperature solution is more appropriate when there is, for example, complete mixing of the medium through convective transfer. Both solutions are rather idealistic, and the true solution is likely to fall between the two.

of no medium. As one adds absorbing and emitting gases or absorbing, emitting, and scattering particles, the heat flux is reduced from the thin limit, and it's temperature distribution becomes much less non-uniform. In the limit of an optically thick medium, as the medium becomes opaque, the communication from the boundaries is limited to "diffusion" of radiation through the medium. In this limit, addition of scattering and/or absorbing material to the medium inhibits the radiative transfer by effectively increasing the distance the radiation must diffuse before reaching other boundaries.

In a real medium, such as found in a coal combustor, the limiting cases described above do not completely describe the radiant transfer since the optical depth of the medium is a strong function of wavelength. For example, if the medium is an infrared active gas, such as CO_2 and H_2O, then there are spectral ranges where the medium is optically thick and other ranges where the medium is transparent. In the optically thick spectral ranges the radiation diffuses through the medium, coupling the radiation field with the temperature of the gases as radiation is absorbed and re-emitted according to the gas temperature. If non-absorbing scattering particles are added to the medium, with a scattering coefficient that is very broadband, then the transparent spectral ranges are regions of pure scattering. In these regions, the addition of scattering reduces the communication between the boundaries by reflecting the incident radiation.

To see how this spectral character manifests itself in the governing equations, consider the general form of the spectral radiative transfer equation,

$$\nabla\cdot\left[\hat{\Omega}I_\lambda\left(\mathbf{r},\hat{\Omega}\right)\right]+\left(\alpha_\lambda+\sigma_\lambda\right)I_\lambda\left(\mathbf{r},\hat{\Omega}\right)=\alpha_\lambda I_{b\lambda}\left[T\left(\mathbf{r}\right)\right]+\frac{\sigma_\lambda}{4\pi}\int_{4\pi}\Phi_\lambda\left(\hat{\Omega}\cdot\hat{\Omega}'\right)I_\lambda\left(\mathbf{r},\hat{\Omega}'\right)d\Omega'. \tag{1}$$

Here $I_\lambda(\mathbf{r},\hat{\Omega})$ is the spectral radiance at position $\mathbf{r}$ in direction $\hat{\Omega}$ in the medium. The Planck blackbody function, $I_{b\lambda}$, is a function of temperature, $T(\mathbf{r})$, which depends on the position in the medium. The absorption coefficient, α_λ, and scattering coefficient, σ_λ, depend on wavelength, as implied by the subscript λ, but in general also depend on the local temperature of the medium.

The total heat flux vector, $\mathbf{q}$, is defined as the integral of the spectral heat flux vector, $\mathbf{q}_\lambda$ over all wavelengths, so that

$$\mathbf{q}\left(\mathbf{r}\right)=\int_0^\infty\mathbf{q}_\lambda\left(\mathbf{r}\right)d\lambda=\int_0^\infty\int_{4\pi}\hat{\Omega}I_\lambda\left(\mathbf{r},\hat{\Omega}\right)d\Omega d\lambda. \tag{2}$$

In radiative equilibrium, the divergence of the heat flux vector is equal to the volumetric heat generation rate, $g(\mathbf{r})$, or

$$\nabla\cdot\mathbf{q}\left(\mathbf{r}\right)=g\left(\mathbf{r}\right). \tag{3}$$

The volumetric heat generation rate is non-zero, for example, in a medium with exothermic chemical reactions. Alternatively, g could be regarded as as the effective net power generation at some position $\mathbf{r}$ arising from all the terms in the energy equation except the net radiative power through a differential volume element per unit volume, $\nabla \cdot \mathbf{q}$. With this interpretation, we regard g as the degree to which the system is out of radiative equilibrium, and treat Eq. (3) as a complete statement of the energy balance throughout the medium where g is a very complicated function including all the convection, conduction, and energy production terms of the full energy equation. In either interpretation, the volumetric power production, g, is not associated with radiative transfer, and does not have a dependence on wavelength.

Since the concern here is the radiative transfer, and not the more complicated full energy balance of the coal combustor, assume that $g(\mathbf{r})$ is specified. By integrating Eq. (1) over all solid angles, Ω, we obtain the equation for the net spectral radiant power at each differential volume element in the medium

$$\nabla \cdot \mathbf{q}_\lambda(\mathbf{r}) + \alpha_\lambda \int_{4\pi} I_\lambda\left(\mathbf{r}, \hat{\Omega}\right) d\Omega = 4\pi\alpha_\lambda I_{b\lambda}\left[T(\mathbf{r})\right] \tag{4}$$

where the identity

$$\frac{1}{4\pi}\int_{4\pi} \Phi_\lambda\left(\hat{\Omega}\cdot\hat{\Omega}'\right) d\Omega \equiv 1 \tag{5}$$

was used to eliminate the in-scattering term in Eq. (1).

Introduce a normalized Planck blackbody function,

$$f_\lambda(T) \equiv \frac{I_{b\lambda}(T)}{\frac{\sigma T^4}{\pi}}, \tag{6}$$

into Eq. (4) and integrate over all wavelengths to obtain

$$\frac{\sigma T^4}{\pi} = \frac{1}{4\pi\bar{\alpha}_P}\left(\nabla\cdot\mathbf{q}(\mathbf{r}) + \int_{4\pi}\int_0^\infty \alpha_\lambda I_\lambda\left(\mathbf{r},\hat{\Omega}\right) d\lambda d\Omega\right). \tag{7}$$

Here $\bar{\alpha}_P$ is the Planck mean absorption coefficient,

$$\bar{\alpha}_P \equiv \int_0^\infty \alpha_\lambda f_\lambda d\lambda. \tag{8}$$

Replace the divergence of the heat flux vector with g in Eq. (7), replace $I_{b\lambda}$ using Eq. (6), and substitute into Eq. (1) to get the alternative formulation of the radiative transport equation

$$\begin{aligned}&\nabla\cdot\left[\hat{\Omega} I_\lambda\left(\mathbf{r},\hat{\Omega}\right)\right] + \left(\alpha_\lambda+\sigma_\lambda\right) I_\lambda\left(\mathbf{r},\hat{\Omega}\right)\\ &= \frac{\alpha_\lambda f_\lambda}{4\pi\bar{\alpha}_P}\left(g(\mathbf{r}) + \int_{4\pi}\int_0^\infty \alpha_{\lambda'} I_{\lambda'}\left(\mathbf{r},\hat{\Omega}'\right) d\Omega' d\lambda'\right) + \frac{\sigma_\lambda}{4\pi}\int_{4\pi}\Phi_{\lambda'}\left(\hat{\Omega}\cdot\hat{\Omega}'\right) I_\lambda\left(\mathbf{r},\hat{\Omega}'\right) d\Omega'.\end{aligned} \tag{9}$$

This formulation has the advantage that the temperature of the medium does not appear explicitly in the equation, but it does appear implicitly, since the radiative properties and f_λ depend on temperature. However, this temperature dependence is often relatively weak, and by solving Eq. (9) iteratively, using Eq. (7) after each iteration to improve the estimates of α_λ, σ_λ, f_λ, and $\bar{\alpha}_P$, the solution will converge.

The equation for the temperature of the medium, Eq. (7), reveals the way in which the spectral characteristics of the medium affect it's temperature. Radiation at wavelengths where α_λ is very small do not contribute to the temperature of the medium, as discussed previously. It is evident that wavelength intervals that contribute significantly to the Planck mean absorption coefficient are the only intervals that affect the temperature.

In practice, it is helpful to replace the continuous spectral formulation presented above with a so–called picket fence model, in which the spectral properties of the medium are assumed to be constant over a finite wavelength interval, $\Delta\lambda$. To obtain this formulation simply integrate the spectral properties over a finite wavelength interval and replace the integrations over λ with summations of a number of wavelength intervals. The resulting equations are

$$\nabla \cdot \left[\hat{\Omega} I_i\left(\mathbf{r},\hat{\Omega}\right)\right] + \left(\alpha_i + \sigma_i\right) I_i\left(\mathbf{r},\hat{\Omega}\right) = \alpha_i f_i \left(\frac{\sigma T^4}{\pi}\right) + \frac{\sigma_i}{4\pi}\int_{4\pi} \Phi_i\left(\hat{\Omega}\cdot\hat{\Omega}'\right) I_i\left(\mathbf{r},\hat{\Omega}'\right) d\Omega' \tag{10}$$

where the subscript i denote the average value over the wavelength interval $\Delta\lambda_i$. The temperature is given by the relation

$$\frac{\sigma T^4}{\pi} = \frac{1}{4\pi\bar{\alpha}_P}\left(g\left(\mathbf{r}\right) + \sum_{i=1}^{N_{\Delta\lambda}} \int_{4\pi} \alpha_i I_i\left(\mathbf{r},\hat{\Omega}\right) d\Omega\right). \tag{11}$$

and the Planck mean absorption coefficient is approximated by

$$\bar{\alpha}_P \equiv \sum_{i=1}^{N_{\Delta\lambda}} \alpha_i f_i. \tag{12}$$

The function f_i now is the blackbody fraction of radiant power in the wavelength interval $\Delta\lambda_i$. Note that as the number of wavelength intervals, $N_{\Delta\lambda}$ approaches infinity this formulation approaches the exact formulation.

2.3.5 Solution and Results

The equations above were re-written for a planar slab and solved approximately using the discrete ordinates method[2] . In addition, computer codes were developed that calculated the spectral absorption coefficient of H_2O and CO_2 using the band models presented in Ludwig et al. [1].

Calculations were done for four test cases with partial pressures of CO_2 and H_2O of 0.16 atm and 0.06 atm respectively. The temperature dependence of the spectral gas absorption coefficient is shown in Fig. 1. Note that this spectral absorption coefficient is not the true spectral absorption coefficient, but is an average value which accurately reproduces the absorption coefficient one would measure for a short path of very low pressure gas using a rather low spectral resolution. In effect, the absorption coefficient used here is the average line strength to line spacing ratio at a given wavelength, and is not corrected (as used here) for line overlap. For the purposes of this work, where the emphasis is on the effects of fly ash on the radiant transfer, it is assumed that the absorption coefficient in Fig. 1 is the true absorption coefficient. This assumption will cause the predicted absorption and emission from the gas to be slightly higher than the true value, since it does not account for the effects of overlapping lines.

The wavelength range from 1 μm to 12.8 μm was divided into 100 finite intervals of equal spacing on a $\log(\lambda)$ scale (i.e., the ratio of neighboring intervals is equal), as shown in Fig. 2. The gas absorption coefficient is averaged over each interval, $\Delta\lambda$ using the formula

$$\bar{\alpha}_\lambda = -\frac{1}{L}\log\left[\frac{1}{\Delta\lambda}\int_{\Delta\lambda} e^{-\alpha_\lambda L}d\lambda\right] \tag{13}$$

where L is the thickness of the slab. This form of averaging is preferred since it effectively weights the absorption coefficient at any given wavelength by it's effect on transmittance. For the small wavelength intervals used here, the averaging is nearly the same as averaging α_λ over the interval, instead of transmittance as in Eq. (13).

The fly ash model used here is one with all the ash having the refractive index of SA05, and with an ash loading $C_{v,\mathrm{STP}} = 5 \times 10^{-6}$. The ash volume fraction at any

2. See previous QPR's for a discussion of the discrete ordinates method.

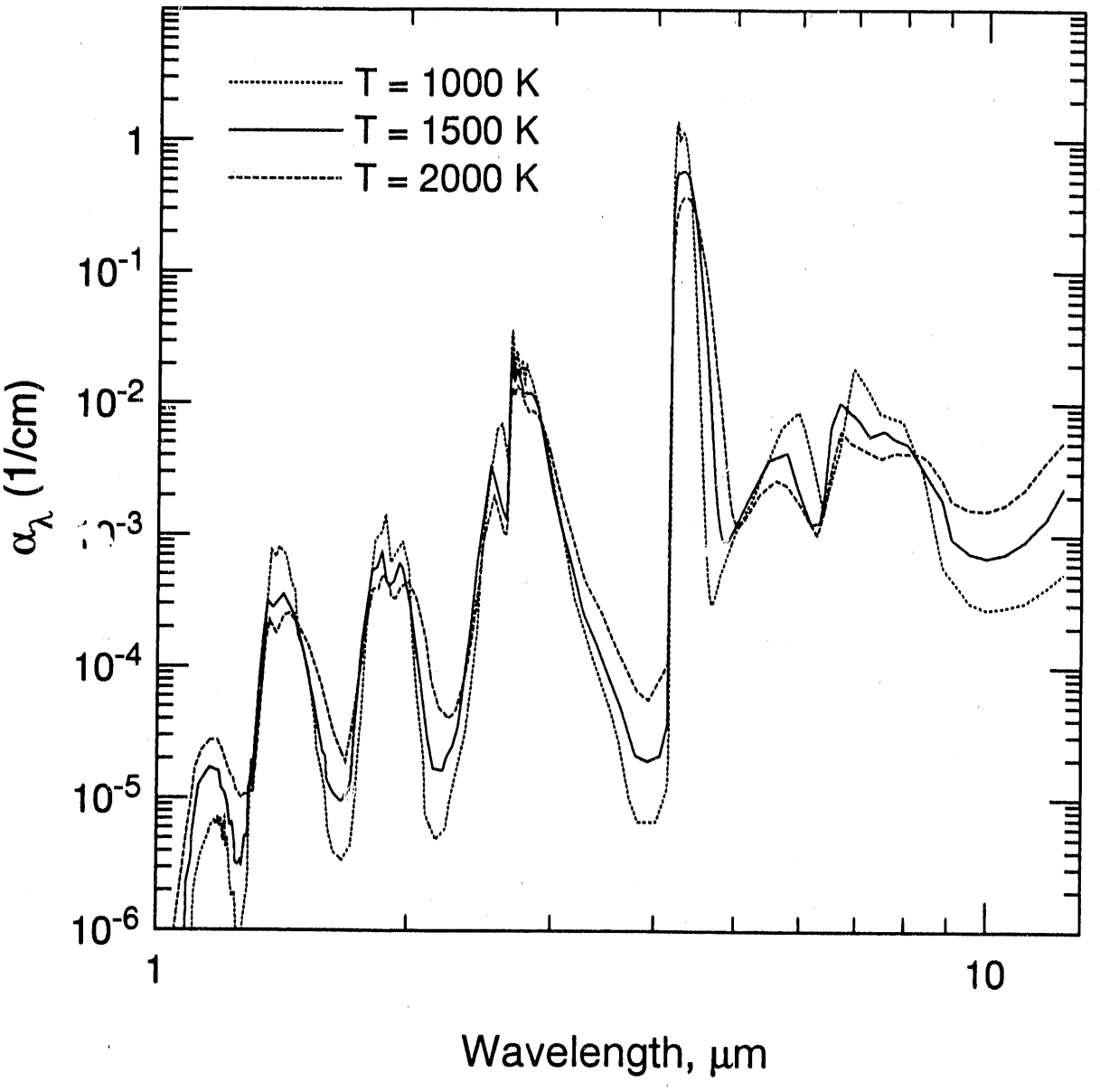

Figure 1: Effect of temperature on the spectral absorption coefficient of a mixture of CO_2 and H_2O with $P_{CO_2} = 0.16$atm and $P_{H_2O} = 0.06$ atm.

temperature and pressure is then computed using the relation

$$C_v(T,P) = C_{v,\mathrm{STP}} \left(\frac{P}{1\mathrm{atm}}\right) \left(\frac{298\mathrm{K}}{T}\right). \tag{14}$$

The temperature distribution for the four cases is shown in Fig. 3. As shown, adding fly ash to the gas causes a significant decrease in the transmittance of the medium,

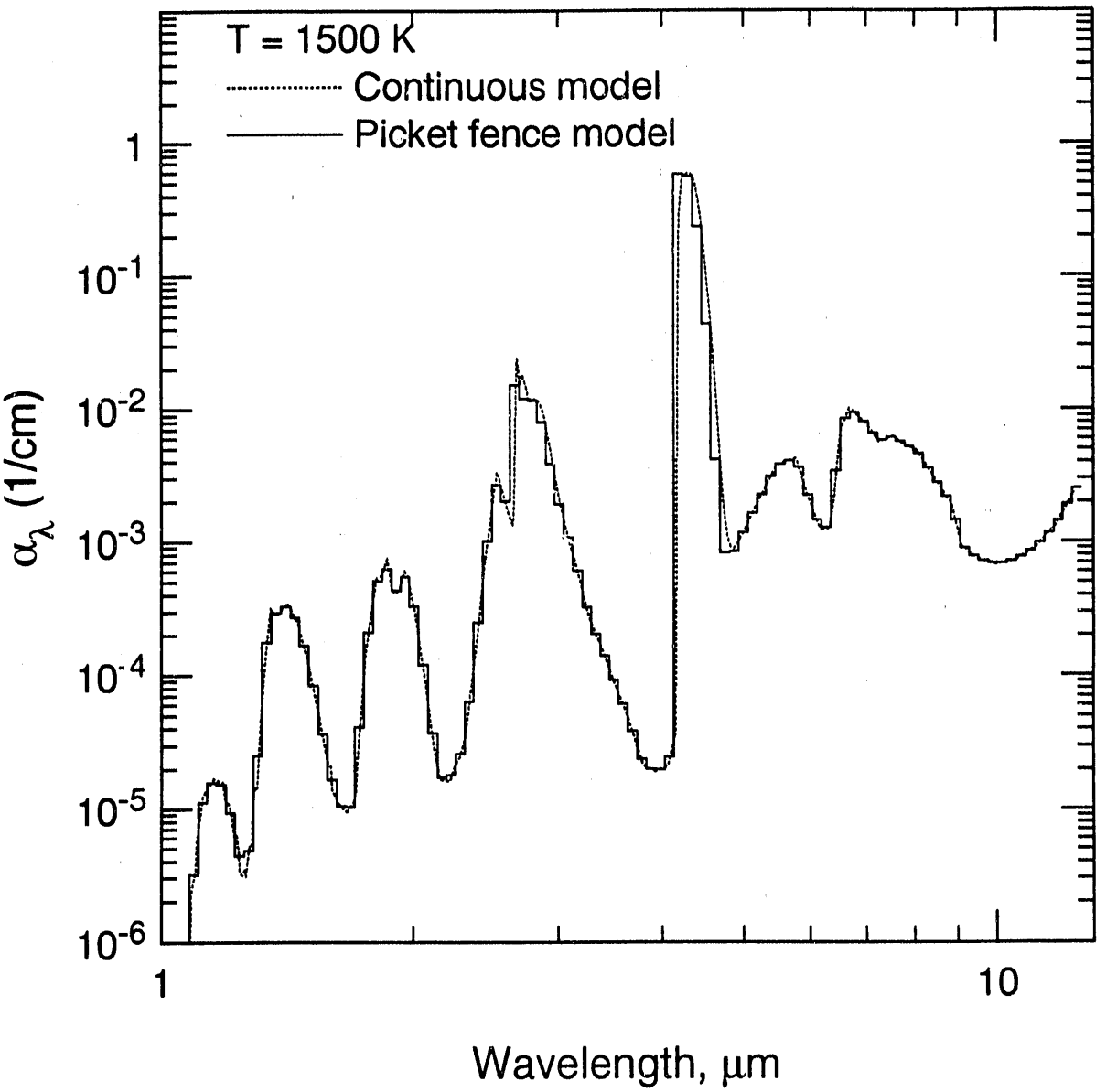

Figure 2: Picket fence model for the gas absorption coefficient for $T = 1500K$, $P_{CO_2} = 0.16$ atm, $P_{H_2O} = 0.06$ atm, and $L = 1$m.

causing the heat flux to decrease. Also, the added optical depth causes the temperature gradient in the medium to increase, as expected.

Finally, it is apparent from the temperature distributions in Fig. 3 that there is an unrealistic oscillation in θ along the distance x/L. The cause of this oscillation is not yet known, but may be due to the fact that the computation was limited to only five

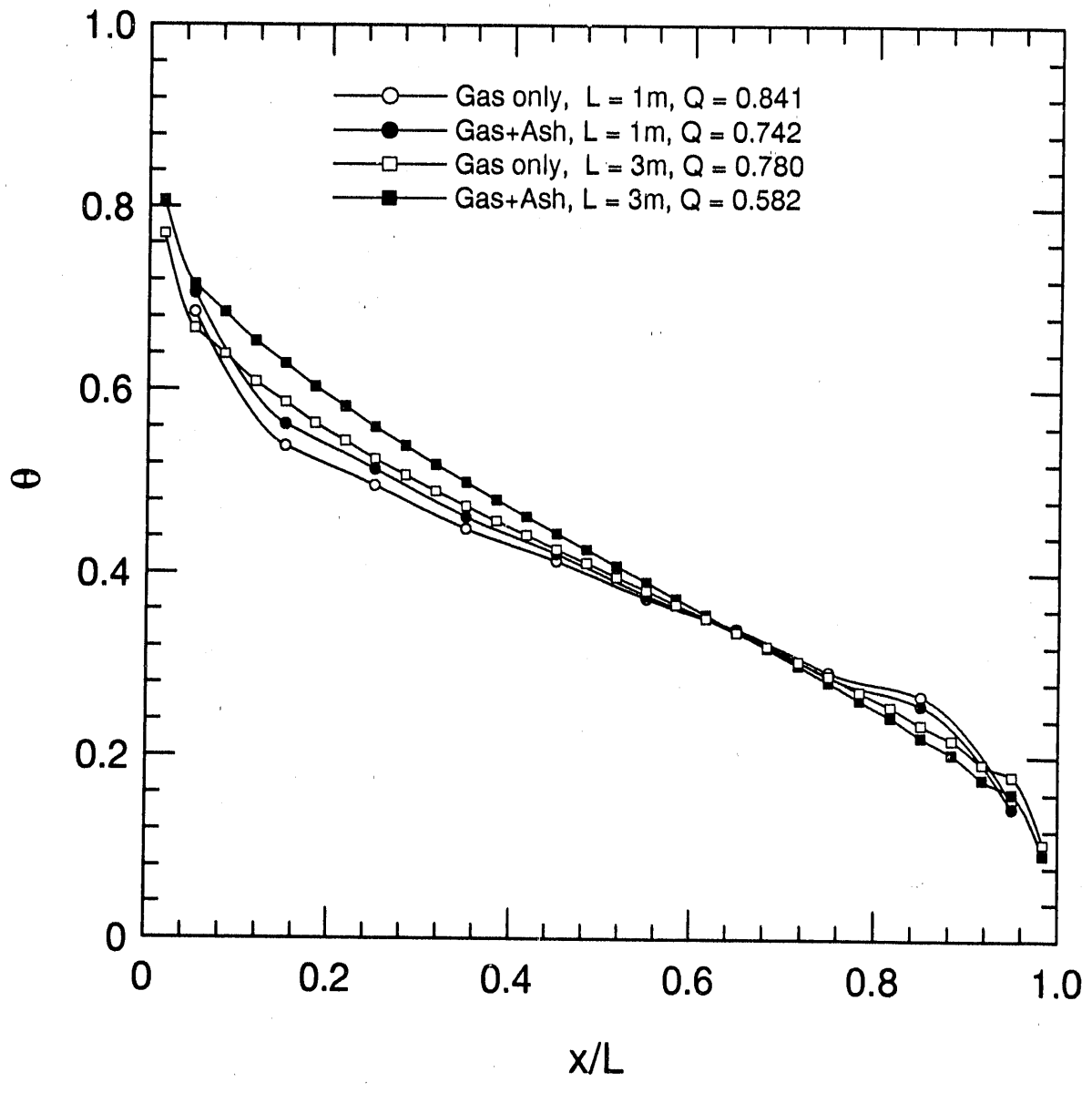

Figure 3: Temperature distribution through medium, as the ratio $\theta = (T^4(x) - T^4(L))/(T^4(0) - T^4(L))$, where $T(L) = 2000$K and $T(0) = 1000$K.

iterations in temperature, so that solutions could be obtained in a reasonable amount of time[3] . During the next quarter the codes will be moved from the IBM PC to a faster

3. Each calculation required approximately 20 hours on a 25 MHz 80386 IBM PC/AT machine with an 80387 math coprocessor

computer so that such time restrictions will vanish. We will then be able to allow the codes to run for many more iterations until a convergent solution is found. Note however that the heat flux, Q, did not show the same oscillations, and is believed to be accurate to within 1%.

2.3.6 Scheduled Activities

During the next quarter the evaluation of the computer code for solving the radiative transfer equation through a medium in radiative equilibrium will continue. The codes will be moved to a faster computer to allow full convergence, as discussed above. Final calculations will be done in preparation for the final report.

2.4 Task 4: Measurement of Radiant Properties of Fly Ash Dispersions

In this Task, a bench-scale experiment under controlled c nditions in the laboratory is to be performed to test the validity of the approach taken in the first three Tasks.

To be specific, the philosophy of our overall approach is the hypothesis that the optical/radiative properties of a particular fly ash dispersion can be predicted by ap ropriate codes (developed under Task 2) using input data on the size and composition distribution of the ash (determined using appropriate microanalytical techniques in Task 1), together with correlations for the spectral and temperature dependence of the complex refractive index as a function of ash composition (determined under Task 3 from measurements on synthetic slags). This fundamental approach has the advantage that the radiative properties of a particular ash (in a particular coal combustion environment) can be predicted purely by characterizing a sample of the ash using established microanalytical techniques, without having to resort to measurements of the optical/radiative properties of each ash, dispersed in a high temperature environment. Such measurements are extremely difficult (or impossible) to perform in a combustion environment, and it is this fact which led us to adopt the present philosophy.

To test the validity of this approach, Task 4 is intended to compare such predictions with measurements of the optical/radiative properties of a dispersion of a representative ash in a bench-style experiment under well-controlled conditions.

As described in past QPRs, a suitable bench-scale experiment has been designed to satisfy the ob jective of Task 4. A major design consideration was the conclusion that there is no known method for dispersing and adequately deagglomerating a sample of ash powder into a gas stream to reproduce the conditions of the ash aerosol before it was collected from the exhaust stream of the coal combustor. This conclusion was based on extensive experience of redispersing ash, and other fine, insulating powders into a gas stream for laboratory research in electrostatic precipitation. On the other hand, we

found that it *is* possible to produce stable, well-deagglomerated dispersions of fly ash in liquids by using ultrasonic agitation. Moreover, by gentle stirring it is possible to maintain stable liquid dispersions at concentrations much higher than is possible with gaseous dispersions. This fact allows one to perform optical extinction and scattering experiments on a much smaller volume of dispersed ash (contained in an optical test cell) than is possible with a gaseous dispersion.

On the basis of an experiment designed around the use of a liquid dispersion, attention was then focused on the choice of liquids and window material for a test cell to allow extinction and/or scattering experiments over the wavelength range of interest, say λ=1–13 μm. While there is no liquid that is transparent over the whole range, it was established that by using three separate liquids, namely carbon tetrachloride (CCl_4), carbon disulfide (CS_2) and bromoform ($CHBr_3$), the full wavelength range could be covered. Moreover, it was also established that there is negligible chemical reaction between fly ash constituents and these liquids. For windows, barium fluoride (BaF_2) is suitable for the range λ=1–13 μm.

In the QPR of February 1991, detailed descriptions of the experimental cell were presented. Mie scattering by particles suspended in a liquid medium was discussed. An alternate optical design of a transmissometer, suitable for our experimental conditions where the path length of the infra-red beam is comparable to the beam diameter, was described. Sensitivity calculations for extinction measurements for fly ash dispersed in CCl_4 were presented in the QPR of April, 1991. In the previous QPR, initial results of reflectance measurements for the real part of the refractive index ($n(\lambda)$) of bromoform and carbon disulfide were presented. The measurements were necessary because spectral values of n were not available for $CHBr_3$. Measurements were also made on CCl_4 and CS_2 to obtain data better resolved spectrally than that available in literature. In this QPR, tabulated results are presented for $n(\lambda)$ of all three liquids. Results of final transmittance measurements on these liquids are presented. Initial results of transmittance measurements on a suspension of Upper Freeport ash is also presented.

Optical Properties of $CHBr_3$, CCl_4, and CS_2:

The spectral refractive index of bromoform and carbon disulfide were presented and discussed in the last QPR, and that of carbon tetrachloride in the QPR of February, 1991. The values of $n(\lambda)$, which we determined for all three liquids, are tabulated in Tables 1, 2, and 3.

Transmittance Measurement Procedure

The schematic for the transmittance measurements is shown in Figure 4. A Nernst Glower, with its ceramic filament operating at an effective blackbody temperature of 1700°C, is used as the broadband radiation source. All the mirrors are gold front surface mirrors. The concave spherical mirrors M1, M3, and M5 each have a focal length of 0.5 m, while the mirrors M2, M4, and M6 are plane. The mirror M1 images the filament at the chopper, which modulates the incident signal at 670 Hz enabling the detector signal to be measured synchronously with a lock-in amplifier. This phase-sensitive detection system eliminates unmodulated background radiation, yielding remarkably good signal/noise ratio, even beyond 11 μm, where the signal intensity is quite low. The image of the filament at the chopper is used as the object for concave mirror M2, which magnifies and images it at the center of the cell. The field stop is adjusted to obtain a circular image. The image at the center of the cell is used as the object for concave mirror which images it at the entrance slit of the monochromator reduced to its original size. Several plane mirrors (M2, M4, M6, M7 and M8) are used to fold the beam. The Ebert-type monochromator is used with multiple sets of gratings to select several spectral ranges. A longpass filter placed at the entrance slit of the monochromator eliminates higher order diffraction inside the monochromator. The detector at the exit slit of the monochromator is a liquid nitrogen cooled, photoconductive HgCdTe infrared detector with a cut-off wavelength of 13 μm. Slit widths of 1 mm are used to allow maximum power to reach the detector while retaining sufficient wavelength resolution. A stepper motor, controlled by the computer, is used to select monochromator dial settings corresponding to desired wavelengths.

Spectrophotometric grade samples of the three liquids (99+%) supplied by Aldrich Chemical Company, Inc. were used for the measurements without further purification. The cell consists of a chamber containing the liquid and an empty control chamber, both having the same BaF_2 windows. Each window is of diameter and thickness 2″ and 3 mm, respectively. BaF_2 is used as the window material because it transmits over the full wavelength range of interest, has a refractive index close to the those of the liquids, does not react with the chemicals, and has very low solubility in water. In conventional transmissometers where the path length is much larger than the beam diameter, a well-collimated beam is used. However, when these two lengths are comparable as in our case, it is found more convenient to use this design where the cell containing the liquid is placed at the image point. A detailed description of the cell design was included in the QPR of February, 1991. The ratio of the signal intensity with the beam passing through the liquid chamber, to that with the beam passing through the empty chamber, is the apparent spectral transmittance, T_{exp}. The correct transmittance is obtained after accounting for reflections at the window-air and window-liquid interfaces and absorption by the windows, as described in the next section.

Calculation of Actual Transmittance of Liquids

The expression for the effective transmittance of a sequence of multiple windows separated by air/vacuum, taking into account the reflectances at the interfaces, and absorption in the windows, is derived in Siegel and Howell (1981). A slightly modified expression is used here because of the presence of the liquid between the windows, although the same nomenclature is used. The dependence of all properties on wavelength is implied throughout, although not shown in order to facilitate easier reading.

If $(T_T)_L$ is the ratio of the energy transmitted through the chamber containing the liquid to energy incident, and $(T_T)_{air}$ is the energy transmitted through the empty chamber, then

$$T_{exp} = \frac{(T_T)_L}{(T_T)_{air}} \tag{1}$$

The denominator is given by

$$(T_T)_{air} = \frac{T_W^2}{1 - R_W^2}$$

Here T_W and R_W are the apparent transmittance and reflectance of one BaF_2 window in air after taking into account multiple reflectance at the two interfaces (i.e., the ratio of the energy transmitted through the window to the energy incident). They are calculated as follows.

$$T_W = \frac{\tau_W (1 - \rho_W)^2}{1 - (\rho_W \tau_W)^2}$$

$$R_W = \rho_W (1 + \frac{\tau_W^2 (1 - \rho_W)^2}{1 - (\rho_W \tau_W)^2})$$

The normal reflectivity, ρ_W, is calculated using the Fresnel relation

$$\rho_W = (\frac{n_W - 1}{n_W + 1})^2 \tag{2}$$

Let T_{WL} and R_{WL} be the apparent transmittance and reflectance of one BaF_2 window with air on the incident side and the liquid on the other. Then

$$T_{WL} = \frac{\tau_W (1 - \rho_W)(1 - \rho_{WL})}{1 - \rho_W \rho_{WL} \tau_W)^2}$$

and

$$R_{WL} = \rho_W + \frac{\tau_W^2 \rho_{WL} (1 - \rho_W)^2}{1 - \rho_W \rho_{WL} \tau_W^2}.$$

The reflectivity of the window-liquid interface, ρ_{WL}, is obtained using the relative refractive index, n_W/n_L, in Equation 2. For the second window, where the incident radiation is on the liquid side, the corresponding apparent reflectance is

$$R_{LW} = \rho_{WL} + \frac{\tau_W^2 \rho_W (1 - \rho_{WL})^2}{1 - \rho_W \rho_{WL} \tau_W^2}$$

The transmittance is symmetric and, hence, $T_{LW} = T_{WL}$ Finally, one can use the above expressions to obtain $(T_T)_L$

$$(T_T)_L = \frac{\tau_L T_L T_{WL}}{1 - \tau_L^2 R_L R_{WL}}$$

Once $(T_T)_L$ is known from Equation 1, the transmittance of the the liquid slab, τ_L, can found solving the quadratic equation shown above.

The spectral refractive index of BaF_2 used in the correction calculations was obtained from Malitson (1964). He used the following Sellmeier-type dispersion equation to fit his data between 0.3 μm and 10.4 μm.

$$n(\lambda)^2 - 1 = \frac{0.643356\ \lambda^2}{\lambda^2 - (0.057789)^2} + \frac{0.506762\ \lambda^2}{\lambda^2 - (0.10968)^2} + \frac{3.8261\ \lambda^2}{\lambda^2 - (46.3864)^2}$$

We used this relation to interpolate and extrapolate to calculate $n(\lambda)$ for the range 1–13 μm (Figure 5). Unfortunately, the effect of the restrahlen absorption band of Ba affects the transmittance (as shown later) beyond 11 μm. Hence, $n(\lambda)$ probably changes more rapidly between 11–13 μm than predicted by the above equation. However, sensitivity calculations showed that the effect of small changes in $n(\lambda)$ of BaF_2 has negligible effect on the calculated transmittance of the liquid.

The transmittance of the window, τ_W, was measured over the wavelength range 1–13 μm. After correction for reflection at the air-window interface, the data is presented in Figure 6. It is seen that the transmittance is greater than 97% upto 10 μm, and that we are operating above the 50% transmission level even at 13 μm.

Transmittance Measurements on CCl_4, CS_2, and $CHBr_3$

The corrected spectral transmittance data for a slab of thickness 9 mm of each of the three liquids are shown in Figure 7. For each liquid, two separate symbols are used to distinguish the transmittance data point before correction, and the data after correction. The liquids used are CCl_4 in the range 1–6 μm, $CHBr_3$ in the ranges 6.0–7.4 μm and 11–13 μm, and CS_2 in the range 7.4–11.0 μm. Clearly, taken together, they provide a window for measurements in the infrared in the wavelength range 1–13 μm. It should be noted that all of the absorption bands shown are weak. However, the transmittance decreases significantly close to the absorption bands because of the relatively large path length of 9 mm. Nevertheless, one can make measurements at specific wavelengths where the liquids are sufficiently transmitting and obtain spectral data over the wavelength range of 1–13 μm. Even when the transmittance of the liquid is low (e.g., bromoform in the 11–13 μm range), the use of chopper and lock-in amplifier with integration times of

3 or 4 seconds yields good signal/noise ratio.

Transmittance Measurements on Fly Ash Suspension These experiments have recently got under way. In previous QPRs, we have discussed the steps taken to maintain a steady signal through an ash suspension over long periods of time. The measured transmittance is the ratio of the signal intensity transmitted through the suspension to that through the clean liquid. Initial results in the near-infrared with Upper Freeport ash suspended in CCl_4 are shown in Figure 8. The volume concentration, V_a, of the ash was 4.0×10^{-5}. The data compares quite closely with sample calculations made previously for SA10 ash. Transmittance measurements over the entire spectral range of interest, and calculations using the bulk composition of Upper Freeport ash are now in progress and will be reported in the next QPR.

Scheduled Activities: Transmittance measurements on fly ash suspensions that were started late in the past quarter will be the main focus of the activities in the upcoming quarter.

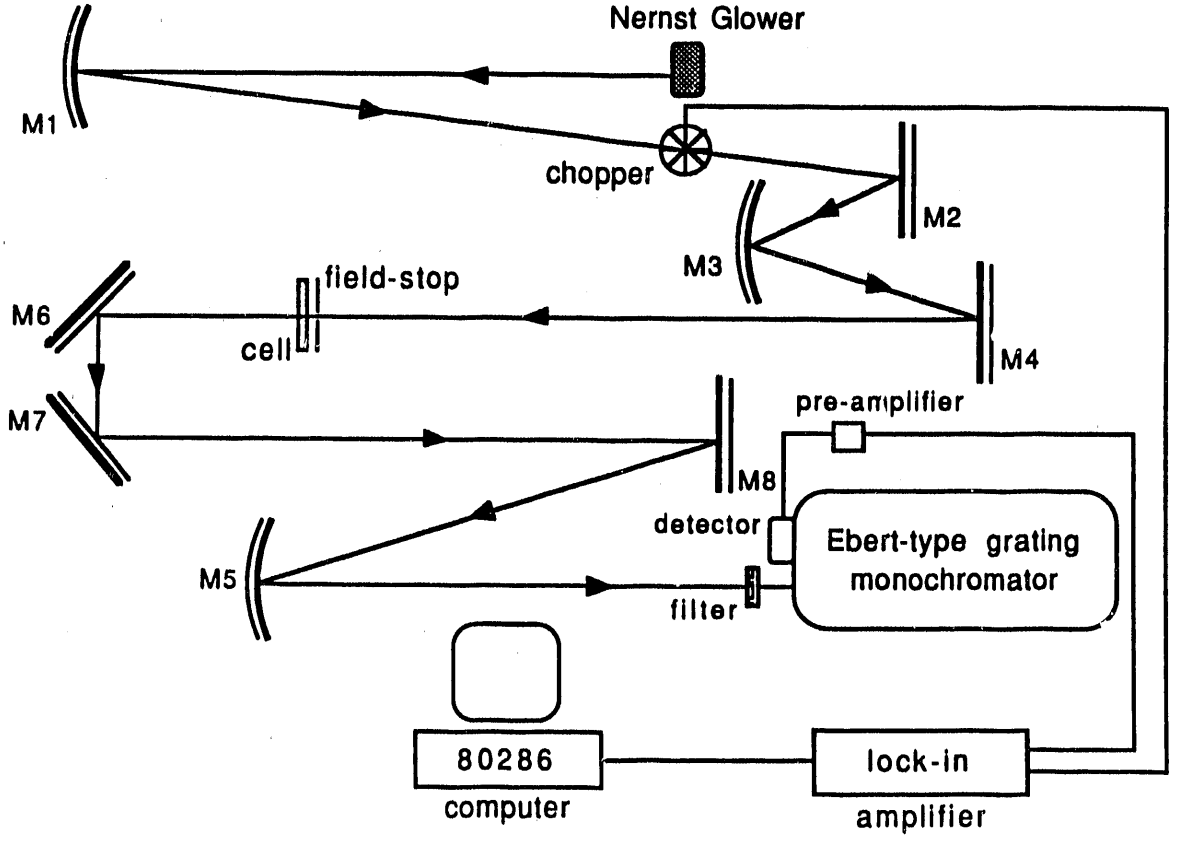

Figure 4. Schematic of Experimental Apparatus for Transmittance Measurements.

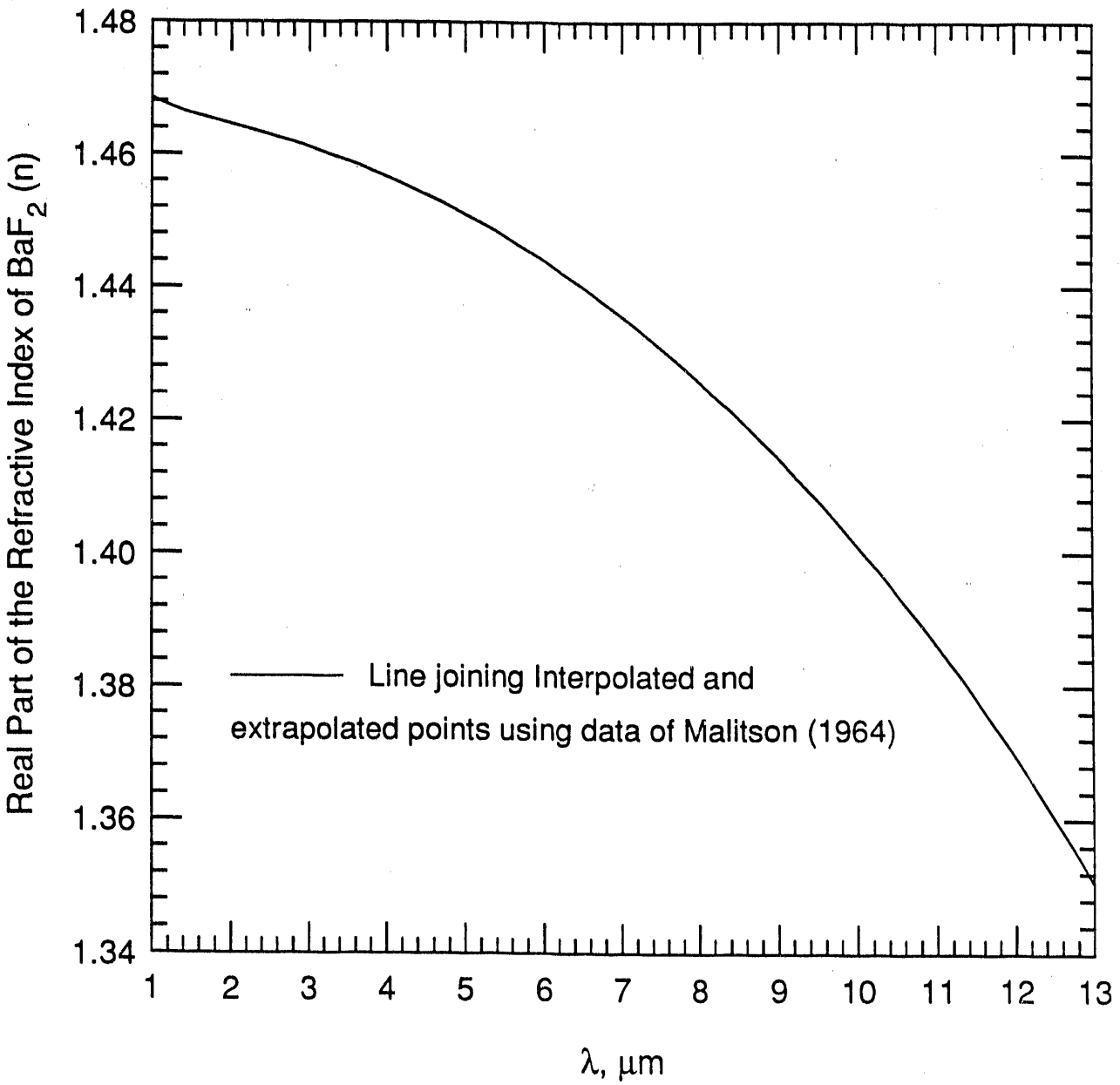

Figure 5. Spectral Refractive Index of Barium Fluoride.

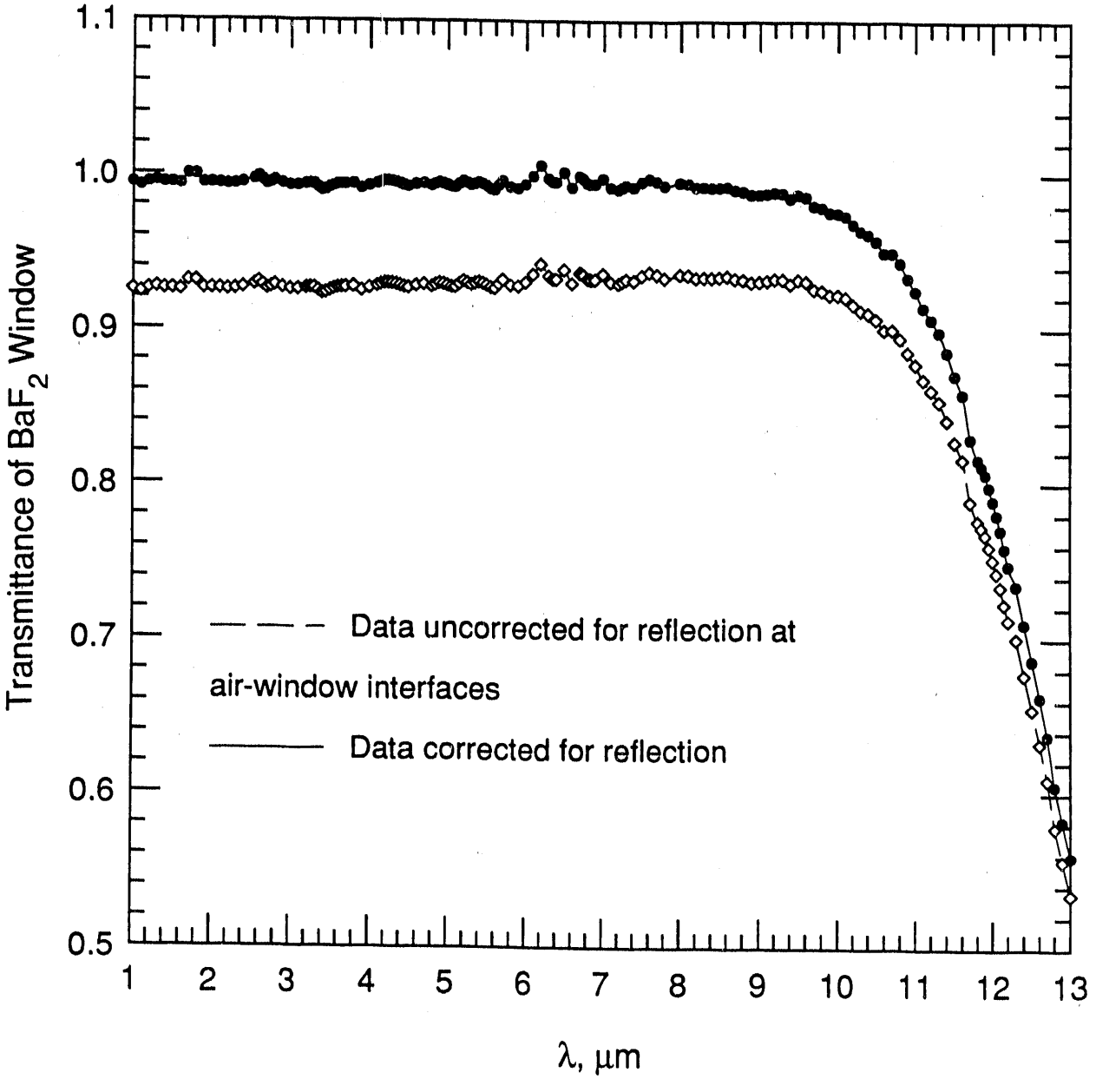

Figure 6. Measured and Corrected Spectral Transmittance of a 3 mm Thick Barium Fluoride Window.

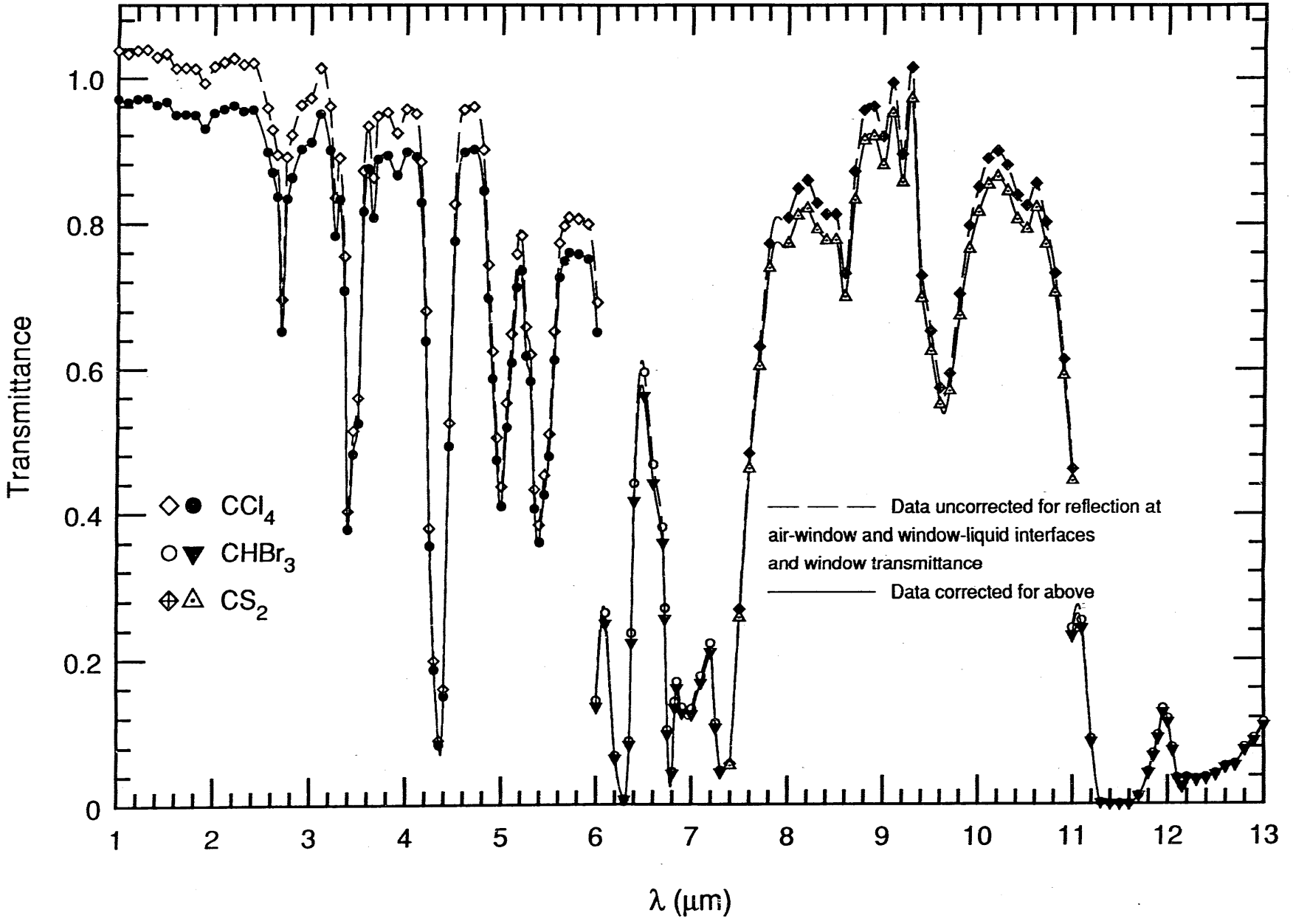

Figure 7. Transmittances of the Three Liquids Over the Selected Wavelength Ranges.

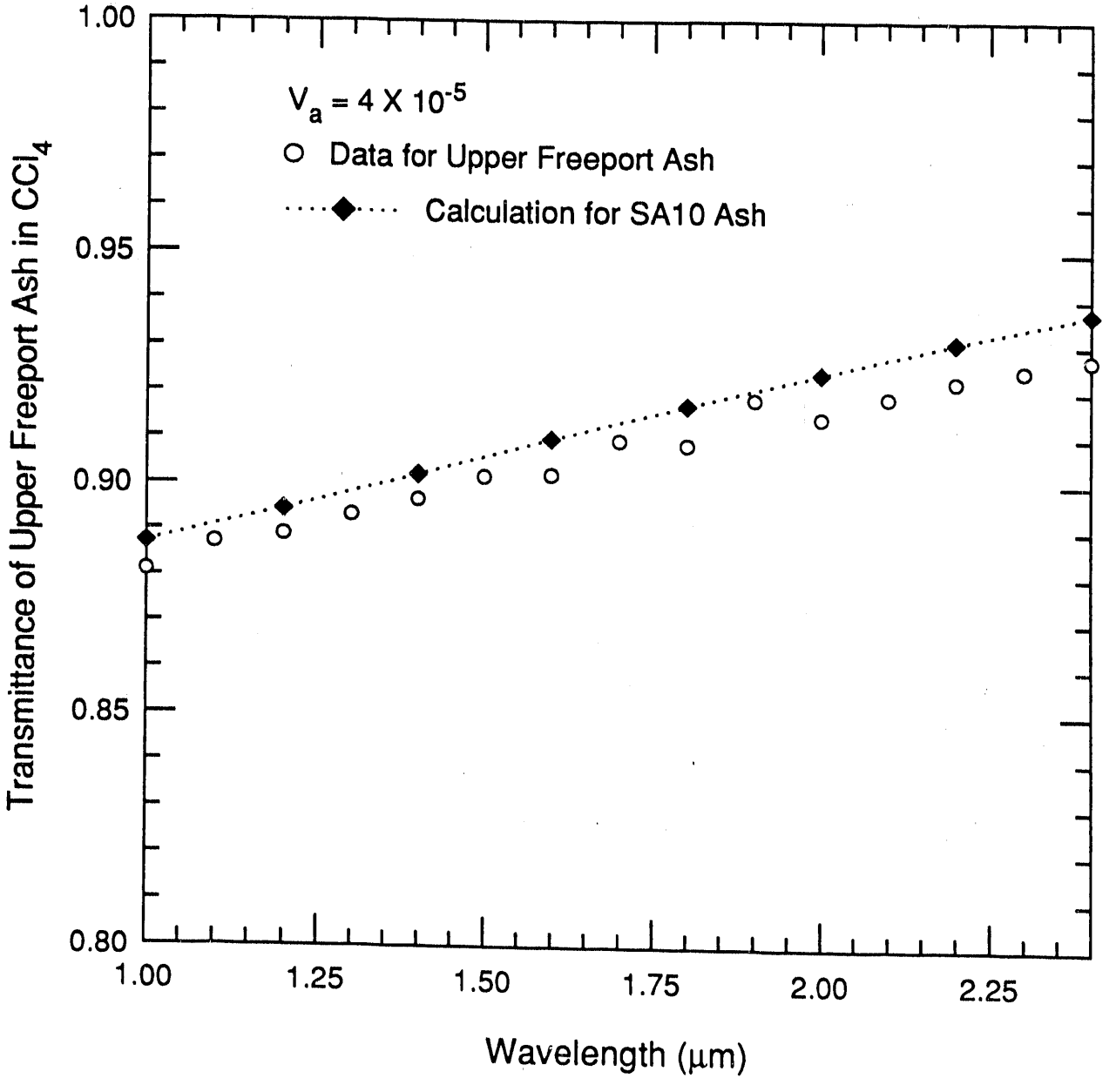

Figure 8. Spectral Transmittance of Upper Freeport Fly Ash Dispersed in Carbon Tetrachloride Compared with Calculations for SA10 ash (D_v = 10 μm, σ_g = 2.5).

Table 1: Spectral Refractive Index of $CHBr_3$, $n(\lambda)$

$\lambda\ (\mu m)$	n	$\lambda\ (\mu m)$	n	$\lambda\ (\mu m)$	n	$\lambda\ (\mu m)$	n
1.0	1.584	3.6	1.572	7.7	1.557	10.0	1.565
1.1	1.583	3.7	1.573	7.8	1.558	10.1	1.565
1.2	1.581	3.8	1.572	7.9	1.556	10.2	1.563
1.25	1.582	3.9	1.573	8.0	1.553	10.3	1.562
1.4	1.581	4.0	1.572	8.1	1.551	10.4	1.560
1.5	1.579	4.1	1.570	8.2	1.548	10.5	1.559
1.6	1.580	4.4	1.569	8.3	1.546	10.6	1.559
1.7	1.576	4.5	1.571	8.4	1.540	10.7	1.557
1.8	1.577	4.6	1.571	8.45	1.536	10.75	1.556
1.9	1.573	4.7	1.569	8.5	1.528	10.8	1.558
2.0	1.578	4.8	1.569	8.55	1.520	10.85	1.554
2.1	1.578	5.0	1.568	8.6	1.505	10.9	1.554
2.2	1.577	5.2	1.564	8.65	1.478	11.0	1.556
2.3	1.576	5.4	1.566	8.7	1.434	11.1	1.550
2.4	1.572	5.5	1.566	8.75	1.458	11.15	1.548
2.5	1.573	5.6	1.565	8.76	1.488	11.2	1.549
2.6	1.571	5.7	1.564	8.78	1.567	11.3	1.544
2.7	1.573	5.8	1.564	8.8	1.649	11.4	1.544
2.8	1.573	6.0	1.565	8.82	1.703	11.5	1.543
3.0	1.573	6.2	1.564	8.84	1.720	11.6	1.543
3.1	1.575	6.25	1.567	8.85	1.719	11.7	1.542
3.2	1.574	6.3	1.565	8.86	1.710	11.8	1.542
3.25	1.572	6.4	1.563	8.9	1.668	11.9	1.540
3.27	1.569	6.45	1.568	8.95	1.635	12.0	1.539
3.275	1.567	6.6	1.564	9.0	1.617	12.1	1.537
3.29	1.566	6.7	1.564	9.1	1.592	12.2	1.532
3.3	1.565	6.9	1.558	9.2	1.584	12.3	1.530
3.31	1.560	7.0	1.564	9.3	1.577	12.4	1.527
3.32	1.571	7.1	1.557	9.4	1.573	12.5	1.526
3.325	1.583	7.2	1.560	9.5	1.569	12.6	1.524
3.33	1.587	7.3	1.562	9.6	1.568	12.7	1.526
3.35	1.582	7.4	1.559	9.7	1.565	12.8	1.522
3.4	1.573	7.5	1.557	9.8	1.564	12.9	1.516
3.5	1.572	7.6	1.559	9.9	1.561	13.0	1.509

Table 2: Spectral Refractive Index of CCl_4, $n(\lambda)$

$\lambda\,(\mu m)$	n	$\lambda\,(\mu m)$	n	$\lambda\,(\mu m)$	n
1.0	1.457	3.6	1.449	6.5	1.436
1.1	1.455	3.7	1.447	6.6	1.435
1.2	1.455	3.8	1.446	6.7	1.430
1.3	1.454	3.9	1.446	6.8	1.435
1.4	1.454	4.0	1.444	6.9	1.427
1.5	1.452	4.1	1.446	7.0	1.430
1.6	1.454	4.2	1.449	7.1	1.429
1.7	1.453	4.4	1.445	7.2	1.431
1.8	1.454	4.5	1.446	7.3	1.429
1.9	1.453	4.6	1.445	7.4	1.429
2.0	1.453	4.7	1.444	7.5	1.427
2.1	1.453	4.8	1.444	7.6	1.426
2.2	1.453	4.9	1.442	7.7	1.426
2.3	1.453	5.0	1.444	7.8	1.424
2.4	1.453	5.1	1.441	7.9	1.423
2.5	1.451	5.2	1.441	8.0	1.420
2.6	1.454	5.3	1.442	8.1	1.423
2.7	1.450	5.4	1.440	8.2	1.420
2.8	1.451	5.5	1.440	8.3	1.421
2.9	1.449	5.6	1.440	8.4	1.420
3.0	1.451	5.8	1.439	8.5	1.419
3.1	1.449	5.9	1.433	8.6	1.416
3.2	1.450	6.0	1.440	8.7	1.416
3.3	1.448	6.2	1.436	8.8	1.413
3.4	1.450	6.3	1.430	8.9	1.414
3.5	1.447	6.4	1.432	9.0	1.410

Table 3: Spectral Refractive Index of CS_2, $n(\lambda)$

$\lambda\,(\mu m)$	n	$\lambda\,(\mu m)$	n	$\lambda\,(\mu m)$	n
7.3	1.740	8.5	1.655	9.7	1.634
7.4	1.710	8.6	1.645	9.8	1.635
7.5	1.697	8.7	1.648	9.9	1.633
7.6	1.683	8.8	1.643	10.0	1.635
7.7	1.680	8.9	1.645	10.2	1.628
7.8	1.674	9.0	1.644	10.3	1.624
7.9	1.671	9.1	1.640	10.4	1.626
8.0	1.663	9.2	1.641	10.5	1.621
8.1	1.667	9.3	1.638	10.6	1.629
8.2	1.657	9.4	1.636	10.7	1.622
8.3	1.660	9.5	1.636	10.8	1.630
8.4	1.651	9.6	1.636	11.0	1.630

References

[1] Ludwig C.B., Malkimus W., Reardon J.E., Thompson J.A.L. *Handbook of Infrared Radiation from Combustion Gases*, NASA SP-3080, 1973.

[2] Malitson I.H. *Refractive Properties of Barium Fluoride*, Journal of Optical Society of America, Vol. 54, No. 5, pp. 628–632, (1964).

[3] Siegel R. and Howell J.R. *Thermal Radiation Heat Transfer*, Second Edition, Hemisphere Publishing Corporation, pp. 722–727, (1981).

END

DATE
FILMED
2/26/92